This is the accepted manuscript made available via CHORUS. The article has been published as:

Charge impurity as a localization center for singlet excitons in single-wall nanotubes

Benjamin O. Tayo and Slava V. Rotkin

Phys. Rev. B **86**, 125431 — Published 20 September 2012

DOI: 10.1103/PhysRevB.86.125431

Charge impurity as a localization center for singlet excitons in single-wall nanotubes

Benjamin O. Tayo[1] and Slava V. Rotkin[1,2]

[1] *Physics Department, Lehigh University, Bethlehem, PA 18015, USA*
[2] *Center for Advanced Materials and Nanotechnology, Lehigh University, Bethlehem, PA 18015, USA*

A simple model is developed for studying the interaction of bright excitons in semiconducting single-wall nanotubes with charged impurities. The model reveals red shift in the energy of excitonic states in the presence of impurity, thus indicating binding of free excitons in the impurity potential well. Several bound states were found in absorption spectrum below the onset of excitonic optical transitions in the bare nanotube. Dependence of the binding energy on the model parameters, such as impurity charge and position, was determined and analytical fits were derived for a number of tubes of different diameter. The nanotube family splitting is seen in the diameter dependence, gradually decreasing with the diameter. By calculating the partial absorption coefficient for a small segment of nanotube, the local nature of the wave function of the bound states was derived.

I. INTRODUCTION

Single-wall nanotubes (SWNTs), tiny hollow cylinders of rolled up graphene sheets, are quasi-one-dimensional (quasi-1D) structures, since their diameter, in the range of one nanometer, is much smaller than the length, up to several hundred micrometers.[1–3] Thus Coulomb interaction, enhanced in 1D, determines their electronic and optical properties. The Coulomb interactions (many-body effects) in SWNTs lead to band gap renormalization[4] and formation of strongly correlated electron-hole pairs, i.e., excitons,[5–7] with binding energies of the order of several hundred meV, much greater than in typical bulk (3D) semiconductors. Solid understanding of the optical properties of SWNTs may allow multiple applications in nanoscale electronics and nanophotonics, making them viable candidates for next-generation nanoscale optoelectronics.[8–13]

Both theoretical calculations and experimental measurements confirm that the optical properties of SWNTs are dominated by excitonic effects. Different theoretical approaches have been used to investigate excitons in SWNTs, including the variational solution[14], or Bloch equation method combined with the tight-binding approximation (TBA) for nanotube single-electron band structure.[6] The most precision was achieved within *ab initio* approach combining the solution of the Bethe-Salpeter (BS) equation with DFT GW-correlated quasiparticle energies.[15,16] The crucial role of excitons for SWNT absorption was confirmed in two-photon experiments in 2005.[17,18] Since then the experimental studies on excitons were extensive.[19–23] Various excitonic interactions, such as exciton-phonon coupling,[24,25] exciton-plasmon coupling,[26] interaction with external electric and magnetic fields[27,28] have been investigated. Most recently the focus of research was on the interactions of excitons with a single charge of mobile (or localized) electron/hole (thus forming a mobile or localized three-body trion) and exciton interactions with a point charge impurity ions.[29–32] The latter is also subject of our work. A fundamental theory of the electronic and optical properties of semiconductors shows importance of impurities, which are often unavoidable and can alter intrinsic properties of semiconductor materials substantially. The single-layer structure of SWNTs makes them extremely sensitive to the surrounding conditions and provides a route for electronic doping via adsorption of molecules with higher (or lower) electron affinity. This can produce drastic changes in their optical properties.[33–36] While the subject of impurity doping is well understood in bulk semiconductors, the role and impact of doping in low dimensional materials like carbon nanotubes is still under investigation, and nature of electronic impurity levels in single-walled carbon nanotubes associated with adatoms is not fully understood yet.

In this paper, we present a model for interaction of excitons with an immobile charge impurity adsorbed on a semiconducting SWNT. We demonstrate that this interaction can induce exciton localization. We show that for a given SWNT, the degree of localization, as indicated by the red shift of the excitonic energy level in a local vicinity of the impurity, depends on the effective charge (effective valency) of the impurity ion, $Z|e|$, and the distance between the ion and SWNT, d. Corresponding scaling laws with Z and d will be derived.

The model can be applied to several cases, for example, to describe SWNT interacting with charged molecules/atoms adsorbed on its surface[37,38] or nanotube-lanthanide ion complexes in solutions.[39] It is known that the ssDNA-wrapped tubes carry a significant surface charge[40–42] due to ionization of the DNA backbone. Thus the model can be relevant for interpretation of the optical shift of the excitonic frequency for the SWNTs coated with DNA[43] (or other ionic polymer[44] or surfactant[45]), the effect formerly attributed to unspecified solvatochromism.[46–49] We speculate that the model can be also applicable to SWNTs placed on a silica substrate, as in the vast majority of optoelectronic devices, because of significant density of the surface states of silica which are readily ionized under ambient conditions. The model should also apply to certain cases of SWNT chemical functionalization. For example, divalent covalent bonding was shown to preserve original pi-band structure of the SWNT while adding charge groups placed

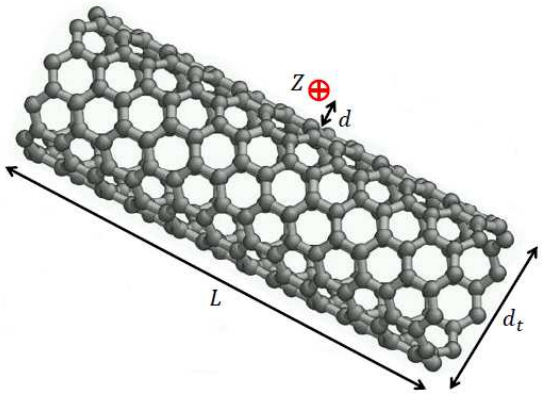

FIG. 1. Schematic representation of the system of a SWNT interacting with a charged impurity. For a given tube with the length, L, and diameter, d_t, the model parameters include the effective charge of the impurity ion, Z, and the position of the ion, $\mathbf{r_p}$.

very close to its surface[50].

This paper is organized as follows: In Sec. II, we develop the theory of impurity scattering of excitons in single-wall carbon nanotubes. In Sec. III, we provide the solution for exciton scattering equation and discuss numerical results. In Sec. IV, we study the optical absorption spectrum of carbon nanotubes in the presence of charged impurities. A short summary concludes the paper.

II. GENERAL FORMALISM

We consider a SWNT of finite length, L, and diameter, d_t, whose excitations are dominated by correlated electron-hole pairs (excitons), interacting with an impurity ion with the effective charge $Z|e|$ (Z being the effective valency of the ion) placed at a distance d above the surface of the SWNT, as shown in Fig. 1. In our model, we treat the potential of an impurity ion as a point charge perturbation to the excitons in the pristine SWNT. That is, we assume that the polarization of the single-particle electron and hole states of the pristine SWNT due to impurity ion is negligible so one can use the same single-particle wave functions even in the presence of the impurity. Explicit form of the single-particle wave functions is given in the Appendix in Eq. (A2). The total two-body Hamiltonian of the system, including perturbation, may be expressed as[51]

$$H = H_{BS} + H_{int} \tag{1}$$

where $H_{BS} = D + 2K_x - K_d$ is the bare Hamiltonian, which has translational symmetry of the SWNT lattice. The diagonal term $D = E_c - E_v$, is the sum of the quasi-particle energies for the uncorrelated electron-hole pair, while K_x and K_d are the exchange and direct Coulomb interaction matrices[52–54].

The operator of interaction is:

$$H_{int}(\mathbf{r}_e, \mathbf{r}_h) = \frac{Ze^2}{|\mathbf{r}_h - \mathbf{r_p}|} - \frac{Ze^2}{|\mathbf{r}_e - \mathbf{r_p}|} \tag{2}$$

here $\mathbf{r}_e$ and $\mathbf{r}_h$ refer to the position vector of the electron and hole, respectively; while $\mathbf{r_p}$ refers to the position of the impurity ion. Since the interaction potential includes both electron and hole symmetrically and we also assume electron-hole symmetry in single-particle band structure, the model gives the same magnitude of perturbation for both positively and negatively charged impurity. Furthermore, in the second order of perturbation theory implemented below, the exciton binding energy is the same for either sign of the ion charge.[55]

It is more convenient to solve Eq. (1) in momentum space. Then the BS equation can be written as[53]

$$H_{BS} A^{(n)}_{\alpha,Q}(k) = \Omega^{(n)}_{\alpha}(Q) A^{(n)}_{\alpha,Q}(k) \tag{3}$$

here $\Omega^{(n)}_{\alpha}(Q)$ is the energy of the nth excitation, α is the quantum number distinguishing bright (B) and dark (D) excitons, Q is the center of mass momentum, and $A^{(n)}_{\alpha,Q}(k)$ is the excitonic wave function in the momentum representation. We consider only excitons with zero total angular momentum which form the lowest energy manyfold[56,57]. More rigorous analysis of spin-singlet excitons includes also a doublet state of an exciton with non-zero total angular momentum (E-symmetry) in addition to A_1 and A_2 states, the dark (valley-antisymmetric) and bright (valley-symmetric) states. In the coordinate space the exciton wave function, as a solution of the bare BS equation, can be expressed as a linear combination of the products of the single-particle electron-hole wave functions:

$$\Phi^{(n)}_{\alpha,Q}(\mathbf{r}_e, \mathbf{r}_h) = \sum_k A^{(n)}_{\alpha,Q}(k) \Big[\psi_{c\mu k+Q}(\mathbf{r}_e) \psi^*_{v\mu k}(\mathbf{r}_h) + \\ + (-1)^{\alpha} \psi_{c\bar{\mu} k+Q}(\mathbf{r}_e) \psi^*_{v\bar{\mu} k}(\mathbf{r}_h) \Big] \tag{4}$$

here $\alpha = 0/1$ corresponds to the bright/dark state and the functions $\psi_{c\mu k}(\mathbf{r})$ are single-particle wave functions, given in Appendix.

In the presence of the impurity, one has to solve the scattering problem. The scattered state can be expressed as

$$\Psi^{(i)}(\mathbf{r}_e, \mathbf{r}_h) = \sum_{n\alpha Q} \mathcal{C}^{(i)}_{\alpha n Q} \Phi^{(n)}_{\alpha,Q}(\mathbf{r}_e, \mathbf{r}_h) \tag{5}$$

where the wave function amplitudes $\mathcal{C}^{(i)}_{\alpha n Q}$ must satisfy Eq. (1). In the momentum space it reads as:

$$\Big[\Omega^{(n')}_{\alpha'}(Q') \delta_{nn'} \delta_{\alpha\alpha'} \delta_{QQ'} + S^{nn'}_{\alpha,\alpha'}(Q, Q') \Big] \mathcal{C}^{(i)}_{\alpha' n' Q'} \\ = E^{(i)} \mathcal{C}^{(i)}_{\alpha n Q} \tag{6}$$

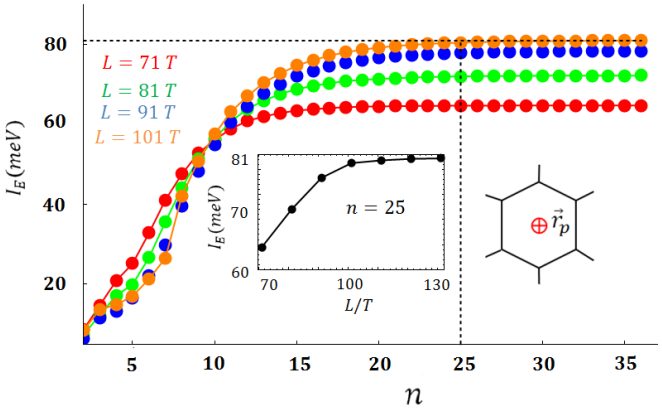

FIG. 2. Convergence of the exciton binding energy, I_E, as a function of the number of included exciton bands, n, for different lengths of (11,0) SWNT computed for $d = 2$ Å and $Z = 3$, with the impurity position ($\mathbf{r_p}$) at the center of the hexagon: (red) $L = 71T$, (green) $L = 81T$, (blue) $L = 91T$, (orange) $L = 101T$, where $T = 0.43$ nm is the unit cell length. Inset panel presents the convergence of the exciton binding energy with respect to SWNT length, L, for $n = 25$.

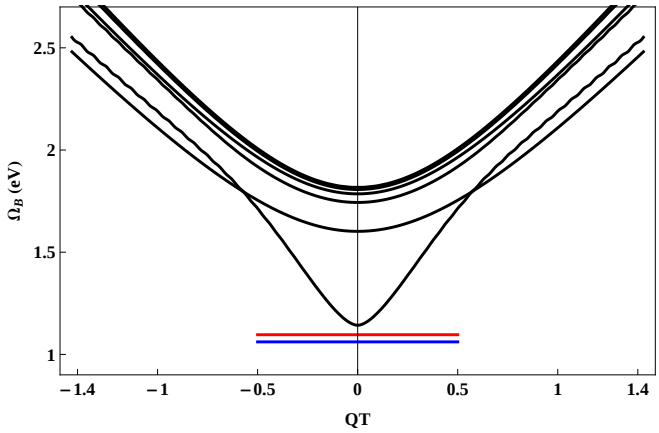

FIG. 3. Exciton energy for an (11,0) SWNT plotted as a function of the dimensionless momentum QT. The horizontal bars represent localized states with binding energies $E_b = 81$ meV and $E_b = 46$ meV calculated for $d = 2$ Å and $Z = 3$.

with the matrix elements $S^{nn'}_{\alpha,\alpha'}(Q,Q')$ given by

$$S^{nn'}_{\alpha,\alpha'}(Q,Q') = \langle \Phi^{(n)}_{\alpha,Q} | H_{int} | \Phi^{(n')}_{\alpha',Q'} \rangle \quad (7)$$
$$= \int d\mathbf{r}_e d\mathbf{r}_h \Phi^{(n)*}_{\alpha,Q}(\mathbf{r}_e,\mathbf{r}_h) H_{int}(\mathbf{r}_e,\mathbf{r}_h) \Phi^{(n')}_{\alpha',Q'}(\mathbf{r}_e,\mathbf{r}_h)$$

In principle, the eigenstates, labeled with the new quantum number i, represent scattered states of perturbed continuum as well as bound states, localized near the impurity as we will show below.

The impurity binding energy for the ith scattered state, $I^{(i)}_E$, is defined as the difference with the energy level of the lowest state of unperturbed bright exciton ($n = 1$):

$$I^{(i)}_E = E^{(i)} - \Omega^{(1)}_B(0) \quad (8)$$

In what follows, we focus on the binding energy of the lowest scattered state ($i = 1$) and for shortcut notations we use below: $I_E \equiv I^{(1)}_E$.

III. NUMERICAL SOLUTION OF THE IMPURITY EQUATION AND DISCUSSION OF THE RESULTS

The task of solving Eq. (6) can be very formidable. However, a few approximations can help to reduce the computational burden. For spin-singlet excitons with zero total angular momentum, the Hilbert space of solutions of the BS equation consist of the bright (valley-symmetric) and dark (valley-antisymmetric) subspaces. The interaction Hamiltonian does not couple bright and dark exciton manifolds (as derived in Appendix). Thus one can solve Eq. (6) separately for the bright and dark manifolds and $S^{nn'}_{\alpha,\alpha'}(Q,Q')$ is diagonal in α,α' indexes. Still, even in the subspace of bright states, the matrix $S^{nn'}_{BB}(Q,Q')$ can be very large since it includes a number of excitonic states with different Q and n quantum numbers.

In order to calculate the energy of the lowest state and I_E in the most efficient way we have to reduce the size of $S^{nn'}$ matrix. We compute $I_E(n)$ as a function of the $n-$cut off, and increase n until we reach convergence, as illustrated in Fig. 2 for a (11,0) SWNT. Same convergence was obtained for $Q-$cut off. Since we performed our calculations for a finite length nanotube, we ensure the stability of numerical results with changing the length of the system. For this particular example of (11,0) SWNT a cut off length of $L = 101T$ (where $T = 0.43$ nm is the unit cell length) and a cut off number of bands of $n = 25$ allowed us to achieve convergence for the exciton binding energy.

Fig. 3 shows the exciton dispersion for pristine (11,0) SWNT together with the impurity induced bound states with binding energies $E_b = 81$ meV and $E_b = 46$ meV calculated for $d = 2$ Å and $Z = 3$.

We found pronounced dependence of I_E on the tube diameter, d_t. In Fig. 4, I_E is shown as a function of d_t. All data points branch into two curves for two different families $r = \mathrm{Mod}(2\mathrm{n} + \mathrm{m}, 3)$ of zigzag tubes. The family splitting decreases with increasing d_t, as well as the overall magnitude of I_E. This can be due to decreasing SWNT curvature or due to the total dipole matrix element (with respect to the ion position above the SWNT surface) which decreases with increasing nanotube size. In order to further investigate this we performed detailed analysis of the behavior of I_E with varying position of the impurity (and also its charge) for the fixed value of d_t.

For a given SWNT, the interaction Hamiltonian H_{int} given by Eq. (2) depends parametrically on Z and $\mathbf{r}_p = \hat{x}(R+d)\cos\theta + \hat{y}(R+d)\sin\theta + \hat{z}z$. Dependence of I_E

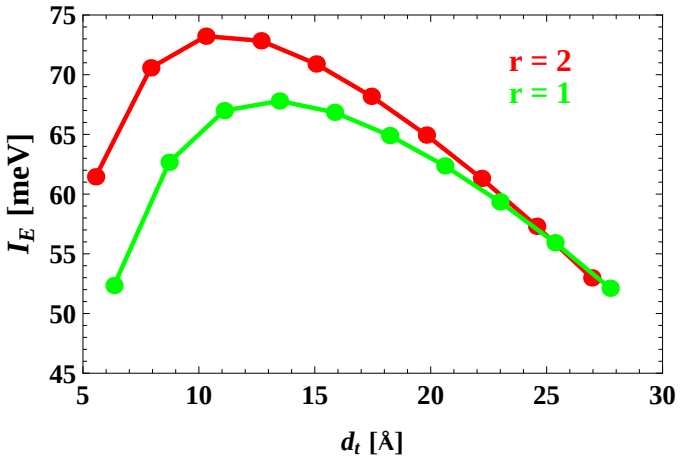

FIG. 4. Exciton binding energy, I_E, as a function of tube diameter, d_t, for the same SWNT-impurity system as shown in Fig. 2. Series of red and green data points correspond to zigzag SWNTs of different families, Mod(2n + m, 3).

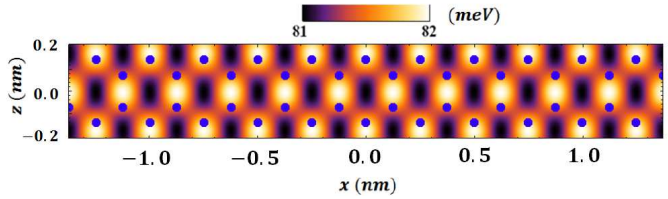

FIG. 5. Exciton binding energy map plotted vs. surface coordinates of the impurity ion for the same SWNT-impurity system as shown in Fig. 2.

TABLE I. Fitting parameters $I_0, d_0, A\ \alpha$, B and β for several (n,0) tubes. I_0 and d_0 are fitted in the range 2 Å $\leq d \leq$ 20 Å for $Z = 3$; A and α are computed using $d = 3$ Å; while B and β are computed for $Z = 3$ and fitted for $d \geq 22$ Å.

tube	$d_t(nm)$	I_0 (eV)	d_0 (Å)	A (meV)	α	B (meV)	β
(8,0)	0.63	0.29	1.71	1.82	3.00	3.78	3.56
(10,0)	0.79	0.25	2.33	3.42	2.71	8.11	3.60
(11,0)	0.87	0.22	2.33	2.94	2.74	4.00	3.58
(13,0)	1.03	0.20	2.89	4.04	2.60	6.98	3.57
(14,0)	1.11	0.19	2.80	3.63	2.63	4.22	3.61
(16,0)	1.27	0.18	3.31	4.07	2.56	5.80	3.48

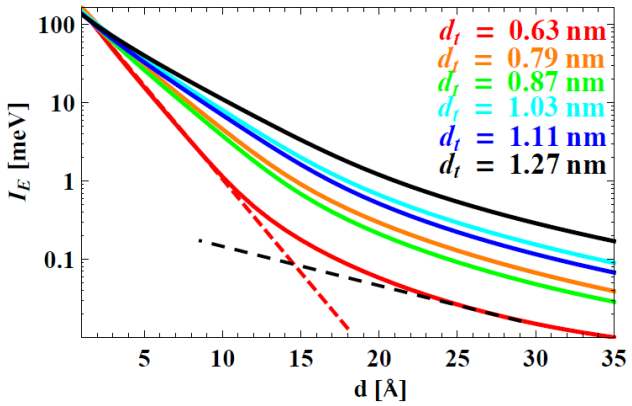

FIG. 6. Exciton binding energy, I_E (log-scale), vs. distance to impurity, d, for few $(n, 0)$ SWNTs and $Z = 3$. Dashed lines show fits in the short- and long-distance limits, Eq. (9,11).

on the latter parameter is expected to be commensurate with the symmetry of the SWNT lattice.

2D map in Fig. 5 presents the variation of the exciton binding energy profile: $I_E(x, z)$, where $x = (R + d)\theta$ is the (curvilinear) surface coordinate of the impurity in the circumferential direction, and z in the axial direction. The $I_E(x, z)$ profile, shown for (11,0) SWNT (within one unwrapped unit cell) for fixed $d = 2$ Å and $Z = 3$, has the maximum when the impurity is right above the center of the carbon bond, and the minimum above the center of the hexagon (as show in the inset of Fig. 2), though the energy difference is negligible, about 1 meV.

Now, we consider the dependence of I_E on d for fixed x, z. Fig. 6 shows the variation of I_E with d for (11,0) SWNT with the ion position shown in the inset of Fig. 2 and $Z = 3$. For small separation from the nanotube wall one can fit the dependence with the exponential function:

$$I_E(d) = I_0 \exp(-d/d_0) \tag{9}$$

where the amplitude, I_0, and the characteristic distance, d_0, vary with the tube diameter, and the effective valency Z. Table I presents the fitting parameters for 6 zigzag SWNTs of different diameters.

This exponential fit of the binding energy works well for the distances 2 Å $\leq d \leq$ 20 Å. Since the perturbation due to a single charged impurity is weak, this is the region of interest to be compared with the experiments. We remark however that for large distances the dipole approximation for the field of the exciton becomes valid. In this approximation, the perturbation due to impurity may be expressed as

$$H_{int} = \frac{-e\mathbf{r} \cdot eZ(\mathbf{R}_{cm} - \mathbf{r_p})}{|\mathbf{R}_{cm} - \mathbf{r_p}|^3} \tag{10}$$

where $\mathbf{r} = \mathbf{r}_e - \mathbf{r_h}$ is the relative coordinate of the exciton, and $\mathbf{R}_{cm} = (\mathbf{r}_e + \mathbf{r_h})/2$ is the center of mass coordinate. Therefore, for large distances the binding energy scales as

$$I_E = B\left(\frac{d_t}{d}\right)^{\beta} \tag{11}$$

The fitting parameters B and β were computed for several SWNTs and the results are summarized in Table I. We can carry out a similar scaling analysis for the dependence of I_E on Z, effective valency of the impurity ion at the fixed ion position. We found the power law dependence

$$I_E(Z) = AZ^{\alpha} \tag{12}$$

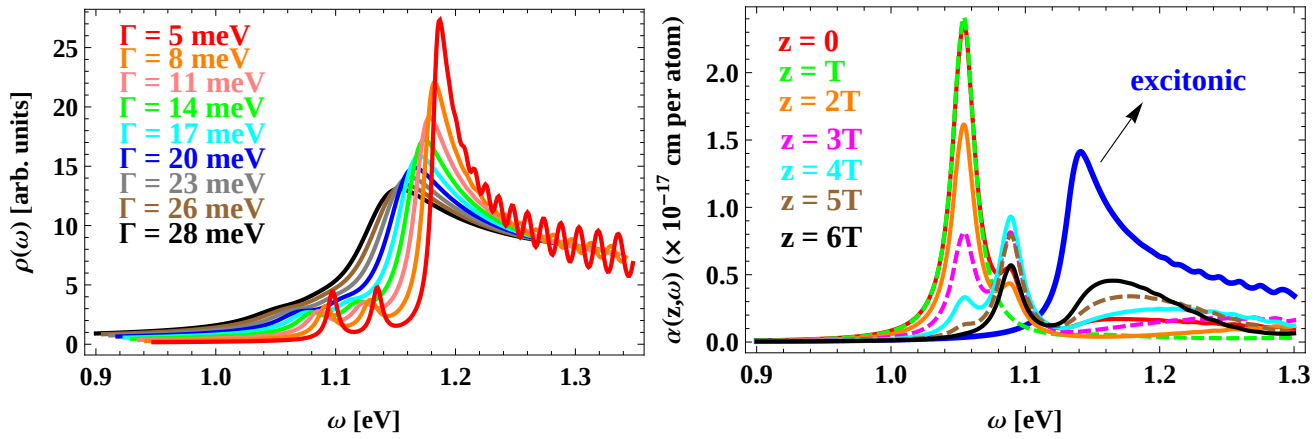

FIG. 7. (Left) $\rho(\omega)$, density of states (offset for clarity) of (11,0) SWNT computed for the same SWNT-impurity system as shown in Fig. 2, plotted for different values of the spectral broadening Γ, shown in the legend (note that the curves are offset for clarity). (Right) Partial absorption coefficient, $\alpha(\omega, z)$, computed with 10 meV broadening: (thick blue) far away from the charged impurity it coincides with the absorption coefficient for the bare SWNT, $\alpha^{(0)}(\omega)$; curves from (black) to (red) show evolution of $\alpha(\omega, z)$ in the local vicinity of the impurity.

The fitting constants A and α are summarized in Table I for zigzag SWNTs for $d = 3$ Å.

IV. OPTICAL SPECTRUM IN THE PRESENCE OF IMPURITY

In order to facilitate comparison of our theoretical predictions with the experiments, we calculate the absorption coefficient of the system, $\alpha(\omega)$.

Within our model we need to include only the states originated from the bright exciton manifold with the wave function of ith eigenstate, given by:

$$\Psi^{(i)}(\mathbf{r}_e, \mathbf{r}_h) = \sum_{nQ} \mathcal{C}^{(i)}_{BnQ} \Phi^{(n)}_{B,Q}(\mathbf{r}_e, \mathbf{r}_h) \qquad (13)$$

Interaction of the excitons with the light of polarization $\vec{\eta}$, is given by the absorption coefficient:[58,59]

$$\alpha(\omega) = \frac{4\pi^2\omega}{\hbar n_b c} \sum_i |M^{(i)}|^2 \delta(\omega - E^{(i)}) \qquad (14)$$

where ω is the photon energy of an incident light, c is the speed of light, n_b is the background refractive index ($n_b = 1$ for air-suspended tubes), $\hbar$ is the reduced Planck constant, and the matrix element is as follows:

$$\begin{aligned} M^{(i)} &= \langle GS|\vec{p}\cdot\vec{\eta}|\Psi^{(i)}\rangle \\ &= \sum_{nQ} \mathcal{C}^{(i)}_{BnQ} M_{nQ} \end{aligned} \qquad (15)$$

here $|GS\rangle$ is the ground state of the SWNT and $\vec{p}$ is the dipole operator. The matrix elements M_{nQ} can be expressed via the dipole matrix elements of the single-particle wave functions:

$$M_{nQ} = \sum_k A^{(n)}_{B,Q}(k) \langle \psi_{c\mu k+Q}|\vec{p}\cdot\vec{\eta}|\psi_{v\mu k}\rangle \qquad (16)$$

In the absence of the impurity, the excitations of the system are solutions of the bare BS equation and Eq. (14) reduces to:[54]

$$\alpha^{(0)}(\omega) = \frac{4\pi^2\omega}{\hbar n_b c} \sum_{nQ} |M_{nQ}|^2 \delta\big(\omega - \Omega^{(n)}_B(Q)\big) \qquad (17)$$

It is very instructive to visualize all scattered excitonic states by plotting the density of states (DOS) because some of those energy levels may have negligible dipole matrix elements. The finite temperature DOS is given by:

$$\rho(\omega) = \sum_i \frac{\Gamma}{(\omega - E^{(i)})^2 + \Gamma^2} \qquad (18)$$

where we replace the Dirac delta function with a Lorentzian with the line width Γ. The DOS for the (11,0) SWNT is shown in Fig. 7 (left) for different line width values of 5 meV $\leq \Gamma \leq$ 28 meV. All curves are offset for clarity. We emphasize that appearing shift of the peak position is solely due to broadening of several neighbor energy states. Two bound levels are clearly seen at $E^{(1)} = 1.054$ eV and $E^{(2)} = 1.089$ eV, both corresponding to the impurity induced localized states, as we prove next.

The absorption of light with $\vec{\eta_z}$ (axial) polarization for the (11,0) SWNT is shown in Fig. 7 (right). Since the total oscillator strength of non-localized excitonic states, integrated along the SWNT length, is larger than the one of the bound state from a single impurity, direct comparison of the total absorption is difficult. Thus we introduce the partial absorption coefficient $\alpha(z, \omega)$. In calculating $\alpha(z, \omega)$ we use the dipole matrix element, integrated out only within a narrow belt with the width $T/4$, containing

one ring of carbon atoms:

$$\alpha(j,\omega) = \frac{4\pi^2\omega}{\hbar n_b c}\sum_i |M^{(i)}(j)|^2\delta(\omega - E^{(i)}) \qquad (19)$$

here j labels the ring position within the finite size SWNT, $-L/2T \le j \le L/2T$. Corresponding matrix element is given by:

$$M^{(i)}(j) = -e\sum_{nQ}\sum_{sk} C^{(i)}_{BnQ} e^{iQ(z_s+jT)} A^{(n)}_{B,Q}(k) \times \\ \times C^{c}_{\mu k+Q}(s)(z_s+jT)C^{v*}_{\mu k}(s) \qquad (20)$$

In the absence of impurity one has to replace $E^{(i)}$ in Eq. (19) with the bare exciton energy $\Omega^{(n)}_B(Q)$, the index of summation $i \to n, Q$ and use bare dipole matrix element given by:

$$M_{nQ}(j) = -e\sum_{sk} e^{iQ(z_s+jT)} A^{(n)}_{B,Q}(k) \times \\ \times C^{c}_{\mu k+Q}(s)(z_s+jT)C^{v*}_{\mu k}(s) \qquad (21)$$

Using the line broadening of 10 meV we plot in Fig. 7, right, the spectrum of the partial absorption along the SWNT axis. The lineshape at large distance from the impurity coincides with the bare absorption spectrum (thick line). At the small distances the same two peaks as in DOS, red shifted from the bare lowest bright exciton position $\Omega^{(1)}_B(0) = 1.135$ eV, show up in the partial absorption. Since these two peaks are below the onset of the bare bright exciton continuum they can be attributed to impurity induced localized states with the binding energies $E_b = 81$ meV and 46 meV respectively. Additional proof of their localization can be presented by visualizing the wave function, or the local optical DOS.

The partial absorption coefficient map or the local optical DOS, shown in Fig. 8 as a function of the photon energy and axial position along the SWNT, has the same low energy spectral features, as seen in Fig. 7. The bound states have very low optical density far away from the impurity position at $z = 0$, with the characteristic localization length of several nm. This is why the partial absorption is almost the same as in the bare SWNT outside the central region.

V. CONCLUSION

In summary, we have shown that a single charged impurity can induce exciton localization in SWNT. The states localized by the impurity can have binding energies ranging from few meV to hundreds of meV depending on the geometry of the actual SWNT-ion complex. We calculated this dependence and parameterized it for three main parameters of the model: the SWNT diameter, d_t, the effective charge of the impurity ion, Z, and the distance of the ion from the surface of the SWNT, d. The binding energy has a weak dependence on the position of the ion on the SWNT surface for the fixed main

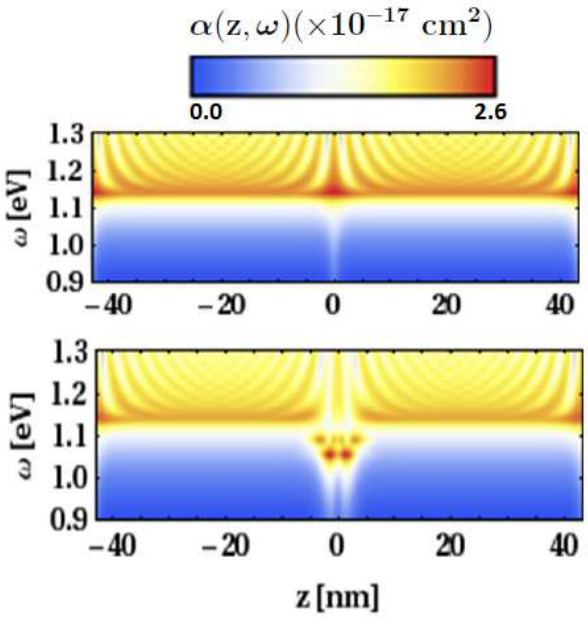

FIG. 8. Map of the partial absorption coefficient (per atom) vs. photon energy, ω, and axial position, z, along the SWNT for the $\vec{\eta_z}$ polarization of light for (11,0) nanotube, $d = 2$ Å and $Z = 3$. (top) for bare SWNT; (bottom) in the presence of impurity at $z = 0$.

parameters. Thus one may expect that in certain cases the impurity could be mobile on the tube surface. By calculating the partial absorption coefficient for a small circular segment of nanotube as a function of the axial coordinate, the local nature of the wave function of the bound states in the vicinity of the impurity was derived. Localization length of the impurity bound exciton can be as small as several nanometers for $Z = 3$, tri-valent ion at the distance $d = 2$ Å from the SWNT surface.

VI. ACKNOWLEDGEMENT

This work was partially supported by National Science Foundation (ECCS-1202398).

Appendix A: Bare exciton wave functions

The excitonic states of non-perturbed Hamiltonian can be written as

$$\Phi^{(n)}_{\alpha,Q}(\mathbf{r}_e,\mathbf{r}_h) = \sum_k A^{(n)}_{\alpha,Q}(k)\Big[\psi_{c\mu k+Q}(\mathbf{r}_e)\psi^*_{v\mu k}(\mathbf{r}_h) + \\ +(-1)^{\alpha}\psi_{c\bar{\mu}k+Q}(\mathbf{r}_e)\psi^*_{v\bar{\mu}k}(\mathbf{r}_h)\Big] \qquad (A1)$$

here $\alpha = 0/1$ corresponds to the bright/dark state and the functions $\psi_{c\mu k}(\mathbf{r})$ are the single-particle wave func-

tions. The latter can be written in tight-binding approximation (TBA) in the form[2]

$$\psi_{\lambda\mu k}(\mathbf{r}) = \sum_{s=1}^{4} C^{\lambda}_{\mu k}(s)\psi_{s\mu k}(\mathbf{r}), \quad \lambda = c, v \tag{A2}$$

as the linear combinations of the Bloch functions $\psi_{s\mu k}(\mathbf{r})$. Using four atoms per unit cell in the SWNT one derives:

$$\psi_{s\mu k}(\mathbf{r}) = \frac{1}{\sqrt{4n}}\frac{1}{\sqrt{N_c}} \sum_{j=-N_c/2}^{N_c/2} \sum_{i'=-n/2}^{n/2} e^{ik(z_s+Tj)} \times \\ \times e^{i\mu(\theta_s+2\pi i'/n)} U(\mathbf{r} - \mathbf{R}_{si'j}) \tag{A3}$$

N_c is the number of unit cells in $(n, 0)$ zigzag SWNT of the finite length, $L = N_c T$, here T is the unit cell length. The coefficients $C^{\lambda}_{\mu k}(s)$ are TBA wave function amplitudes, the function $U(\mathbf{r} - \mathbf{R}_{si'j})$ represents the atomic orbital localized on site $si'j$; k is the axial momentum, defined within the first Brillouin zone:

$$-\frac{\pi}{T} \le k < \frac{\pi}{T} \tag{A4}$$

and μ the azimuthal quantum number, while $\bar{\mu}$ stands for $-\mu$.

Appendix B: Evaluation of matrix elements and detailed derivation of the coupling between bright and dark excitons

For excitons with zero total angular momentum, the Hilbert space of solutions of the BS equation consist of the bright and dark subspaces: $|B\rangle$ and $|D\rangle$. We do not consider E-excitons here because of their non-zero angular momentum quantum number. Then the Hamiltonian, Eq.(1), has the form

$$H = \begin{pmatrix} \Omega_B + S_{BB} & S_{BD} \\ S_{DB} & \Omega_D + S_{DD} \end{pmatrix} \tag{B1}$$

Coupling between bright and dark excitons is described by the matrix element $S^{nn'}_{B,D}(Q, Q')$ which may be expressed as

$$S^{(nn')}_{B,D}(Q, Q') = \sum_{k,k'} A^{*(n)}_{B,Q}(k) A^{(n')}_{D,Q'}(k') \Big[G_{KK} - G_{KK'} + \\ + G_{K'K} - G_{K'K'} \Big] \tag{B2}$$

where

$$G_{KK} = \int d\mathbf{r}_e d\mathbf{r}_h \psi^*_{c\mu k+Q}(\mathbf{r}_e)\psi_{v\mu k}(\mathbf{r}_h) H_{int}(\mathbf{r}_e, \mathbf{r}_h) \times \\ \times \psi_{c\mu k'+Q'}(\mathbf{r}_e)\psi^*_{v\mu k'}(\mathbf{r}_h)$$
$$G_{K'K'} = \int d\mathbf{r}_e d\mathbf{r}_h \psi^*_{c\bar{\mu} k+Q}(\mathbf{r}_e)\psi_{v\bar{\mu} k}(\mathbf{r}_h) H_{int}(\mathbf{r}_e, \mathbf{r}_h) \times \\ \times \psi_{c\bar{\mu} k'+Q'}(\mathbf{r}_e)\psi^*_{v\bar{\mu} k'}(\mathbf{r}_h)$$
$$G_{KK'} = \int d\mathbf{r}_e d\mathbf{r}_h \psi^*_{c\mu k+Q}(\mathbf{r}_e)\psi_{v\mu k}(\mathbf{r}_h) H_{int}(\mathbf{r}_e, \mathbf{r}_h) \times \\ \times \psi_{c\bar{\mu} k'+Q'}(\mathbf{r}_e)\psi^*_{v\bar{\mu} k'}(\mathbf{r}_h)$$
$$G_{K'K} = \int d\mathbf{r}_e d\mathbf{r}_h \psi^*_{c\bar{\mu} k+Q}(\mathbf{r}_e)\psi_{v\bar{\mu} k}(\mathbf{r}_h) H_{int}(\mathbf{r}_e, \mathbf{r}_h) \times \\ \times \psi_{c\mu k'+Q'}(\mathbf{r}_e)\psi^*_{v\mu k'}(\mathbf{r}_h) \tag{B3}$$

In semiconducting SWNTs, there are two degenerate valleys associated with the K and K' points at the corners of the first Brillouin zone, therefore all exciton-impurity scattering states can be expressed in terms of the four G matrix elements. Computation of the matrix elements G_{KK} is greatly simplified if one takes into account the electron-hole symmetry of the interaction Hamiltonian:

$$H_{int}(\mathbf{r}_e, \mathbf{r}_h) = H_h(\mathbf{r_h}) + H_e(\mathbf{r_e}) \tag{B4}$$

where

$$H_h(\mathbf{r_h}) = \frac{Ze^2}{|\mathbf{r}_h - \mathbf{r_p}|}, \quad H_e(\mathbf{r_e}) = -\frac{Ze^2}{|\mathbf{r}_e - \mathbf{r_p}|} \tag{B5}$$

Each term in Eq. (B3) is the sum of two one-body integrals for an electron and for a hole.

Let us compute G_{KK} exactly. We have

$$G_{KK} = \int d\mathbf{r}_e d\mathbf{r}_h \psi^*_{c\mu k+Q}(\mathbf{r}_e)\psi_{v\mu k}(\mathbf{r}_h) H_{int}(\mathbf{r}_e, \mathbf{r}_h) \times \\ \times \psi_{c\mu k'+Q'}(\mathbf{r}_e)\psi^*_{v\mu k'}(\mathbf{r}_h) \\ = \int d\mathbf{r}_h \psi_{v\mu k}(\mathbf{r_h}) H_h(\mathbf{r_h}) \psi^*_{v\mu k'}(\mathbf{r}_h) \times \\ \times \int d\mathbf{r}_e \psi^*_{c\mu k+Q}(\mathbf{r_e})\psi_{c\mu k'+Q'}(\mathbf{r}_e) + \\ - \int d\mathbf{r}_h \psi_{v\mu k}(\mathbf{r_h})\psi^*_{v\mu k'}(\mathbf{r}_h) \times \\ \times \int d\mathbf{r}_e \psi^*_{c\mu k+Q}(\mathbf{r_e}) H_e(\mathbf{r_e}) \psi_{c\mu k'+Q'}(\mathbf{r}_e) \tag{B6}$$

If we neglect the polarization of the one-electron wave functions in the presence of the impurity, then one can use the orthonormality condition of the Bloch functions

$$\int d\mathbf{r}\ \psi_{v\mu k}(\mathbf{r})\psi^*_{v\mu' k'}(\mathbf{r}) = \delta_{\mu,\mu'}\delta_{k,k'} \tag{B7}$$

to simplify the above equation and finally get:

$$G_{KK} = I_h(Q, Q', k, k') - I_e(Q, Q', k, k') \tag{B8}$$

where

$$I_h = \delta_{k+Q,k'+Q'} \int d\mathbf{r}_h \psi_{v\mu k}(\mathbf{r_h}) H_h(\mathbf{r_h}) \psi^*_{v\mu k'}(\mathbf{r}_h)$$
$$I_e = \delta_{k,k'} \int d\mathbf{r}_e \psi^*_{c\mu k+Q}(\mathbf{r_e}) H_e(\mathbf{r_e}) \psi_{c\mu k'+Q'}(\mathbf{r}_e) \quad \text{(B9)}$$

We can proceed in a similar fashion to compute all the matrix elements $G_{K'K'}, G_{K,K'}$ and $G_{K',K}$. It is trivial to show that:

$$G_{K'K'} = G_{KK}, \quad G_{KK'} = G_{K'K} = 0. \quad \text{(B10)}$$

Therefore, this perturbation potential cannot mix the bright and dark states. This means that the Hamiltonian matrix is block-diagonal. For the bright exciton, for example, sought solutions should be obtained from the Hamiltonian:

$$H_B = \Omega_B + S_{BB}, \quad \text{(B11)}$$

while for a dark exciton from:

$$H_D = \Omega_D + S_{DD}. \quad \text{(B12)}$$

[1] S. Iijima, Nature **354**, 56 (1991).
[2] R. Saito, G. Dresselhaus, and M. S. Dresselhaus, *Physical Properties of Carbon Nanotubes* (Imperial College Press, 1998).
[3] S. Reich, C. Thomsen, and J. Maultzsch, *Carbon Nanotubes: Basic Concepts and Physical Properties* (Wiley-VCH, Berlin, 2004).
[4] J. U. Lee, Phys. Rev. B **75**, 075409 (2007).
[5] G. Dukovic, F. Wang, D. Song, M. Sfeir, T. Heinz, and L. Brus, Nano Lett. **5**, 2314 (2005).
[6] E. Malić, M. Hirtschulz, F. Milde, M. Richter, J. Maultzsch, S. Reich, and A. Knorr, Phys. Status Solidi B **245**, 2155 (2008).
[7] T. Ando, J. Phys. Soc. Jpn. **66**, 1066 (1997).
[8] S. V. Rotkin, and S. Subramoney (eds.), *Applied Physics Of Carbon Nanotubes: Fundamentals Of Theory, Optics And Transport Devices* (Springer-Verlag, Berlin, 2005).
[9] A. Jorio, M. S. Dresselhaus, and G. Dresselhaus, *Carbon Nanotubes: Advanced Topics in the Synthesis, Structure, Properties and Application* (Springer, New York, 2008).
[10] F. Xia, M. Steiner, Y. -M. Line, and Ph. Avouris, Nature Nanotech. **3**, 609 (2008).
[11] P. Avouris, M. Freitag, and V. Perebeinos, Nature Photonics **2**, 341 (2008).
[12] J. -H. Han, G. L. C. Paulus, R. Maruyama, D. A. Heller, W. -J. Kim, P. W. Barone, C. Y. Lee, J. H. Choi, M. -H. Ham, C. Song, C. Fantini, and M. S. Strano, Nature Mater. **9**, 833 (2010).
[13] T. Hertel, Nature Photonics **4**, 77 (2010).
[14] T. G. Pedersen, Phys. Rev. B **67**, 073401 (2003).
[15] C. D. Spataru, S. Ismail-Beigi, L. X. Benedict, and S. G. Louie, Phys. Rev. Lett. **92**, 077402 (2004).
[16] E. Chang, G. Bussi, A. Ruini, and E. Molinari, Phys. Rev. B. **72**, 195423 (2005).
[17] F. Wang, G. Dukovic, L. E. Brus, and T. F. Heinz, Science **308**, 838 (2005).
[18] J. Maultzsch, R. Pomraenke, S. Reich, E. Chang, D. Prezzi, A. Ruini, E. Molinari, M. S. Strano, C. Thomsen, and C. Lienau, Phys. Rev. B **72**, 241402(R) (2005).
[19] J. Lefebvre, D. G. Austing, J. Bond, and P. Finnie, Nano Lett. **6**, 1603 (2006).
[20] J. Shaver, J. Kono, O. Portugall, V. Krstić, G. L. J. A. Rikken, Y. Miyauchi, S. Maruyuma, and V. Perebeinos, Nano Lett. **7**, 1851 (2007).
[21] I. B. Mortimer and R. J. Nicholas, Phys. Rev. Lett. **98**, 027404 (2007).
[22] R. Matsunaga, K. Matsuda, and Y. Kanemitsu, Phys. Rev. Lett. **101**, 147404 (2008).
[23] D. M. Harrah, J. R. Schneck, A. A. Green, M. C. Hersam, L. D. Ziegler, and A. K. Swan, ACS Nano **5**, 9898 (2011).
[24] V. Perebeinos, J. Tersoff, and P. Avouris, Phys. Rev. Lett. **94**, 027402 (2005).
[25] F. Plentz, H. B. Ribeiro, A. Jorio, M. S. Strano, and M. A. Pimenta, Phys. Rev. Lett. **95**, 247401 (2005).
[26] I. V. Bondarev, L. M. Woods, and K. Tatur, Phys. Rev. B **80**, 085407 (2009).
[27] V. Perebeinos and P. Avouris, Nano Lett. **7**, 609 (2007).
[28] A. Srivastava, H. Htoon, V. I. Klimov, and J. Kono, Phys. Rev. Lett. **101**, 087402 (2008).
[29] K. Matsuda, Y. Miyauchi, T. Sakashita, and Y. Kanemitsu, Phys. Rev. B **81**, 033409 (2010).
[30] R. Matsunaga, K. Matsuda, and Y. Kanemitsu, Phys. Rev. Lett. **106**, 037404 (2011).
[31] S. M. Santos, B. Yuma, S. Berciaud, J. Shaver, M. Gallart, P. Gilliot, L. Cognet, and B. Lounis, Phys. Rev. Lett. **107**, 187401 (2011).
[32] J. J. Crochet, J. G. Duque, J. H. Werner, and S. K. Doorn, Nature Nanotech. **7**, 126 (2012).
[33] Y. Ohno, S. Iwasaki, Y. Murakami, S. Kishimoto, S. Maruyama, and T. Mizutani, Phys. Rev. B **73**, 235427 (2006).
[34] G. Dukovic, B. E. White, Z. Zhou, F. Wang, S. Jockusch, M. L. Steigerwald, T. F. Heinz, R. A. Friesner, N. J. Turro, and L. E. Brus, J. Am. Chem. Soc. **126**, 15269 (2004).
[35] G. N. Ostojic, S. Zaric, J. Kono, M. S. Strano, V. C. Moore, R. H. Hauge, and R. E. Smalley, Phys. Rev. Lett. **92**, 117402 (2004).
[36] M. Steiner, M. Freitag, V. Perebeinos, A. Naumov, J. P. Small, A. A. Bol, and P. Avouris, Nano Lett. **9**, 3477 (2009).
[37] E. Malic, C. Weber, M. Richter, V. Atalla, T. Klamroth, P. Saalfrank, S. Reich, and A. Knorr, Phys. Rev. Lett. **106**, 097401 (2011).
[38] S. Ghosh, S. M. Bachilo, R. A. Simonette, K. M. Beckingham, and R. B. Weisman, Science **330**, 1656 (2010).
[39] T. Ignatova, H. Najafov, A. Ryasnyanskiy, I. Biaggio, M. Zheng, and S. V. Rotkin, ACS Nano **5**, 6052 (2011).
[40] S. Manohar, T. Tang, and A. Jagota, J. Phys. Chem. C **111**, 17835 (2007).
[41] R. R. Johnson, A. T. Charlie Johnson, and M. L. Klein, Nano Lett. **8**, 69 (2008).
[42] S. V. Rotkin, Annu. Rev. Phys. Chem. **61**, 241 (2010).
[43] H. Qian, P. T. Araujo, C. Georgi, T. Gokus, N. Hartmann, A. A. Green, A. Jorio, M. C. Hersam, L. Novotny, and A. Hartschuh, Nano Lett. **8**, 2706 (2008).
[44] S. -Y. Ju, , J. Doll, I. Sharma, and F. Papadimitrakopoulos, Nature Nanotech. **3**, 356 (2008).
[45] R. Haggenmueller, S. S. Rahatekar, J. A. Fagan, J. Chun, M. L. Becker, R. R. Naik, T. Krauss, L. Carlson, J. F. Kadla, P. C. Trulove, D. F. Fox, H. C. DeLong, Z. Fang, S. O. Kelley, and J. W. Gilman, Langmuir, **24**, 5070 (2008).
[46] J. Lefebvre, J. M. Fraser, Y. Homma, and P. Finnie, Appl. Phys. A: Mater. Sci. Process. **78**, 1107 (2004).
[47] T. Hertel, A. Hagen, V. Talalaev, K. Arnold, F. Hennrich, M. Kappes, S. Rosenthal, J. McBride, H. Ulbricht, and E. Flahaut, Nano Lett. **5**, 511 (2005).
[48] J. H. Choi and M. S. Strano, Appl. Phys. Lett. **90**, 223114 (2007).
[49] C. A. Silvera-Batista, R. K. Wang, P. Weinberg, and K. J. Ziegler, Phys. Chem. Chem. Phys. **12**, 6990 (2010).
[50] D. Bouilly, J. Cabana, F. Meunier, M. Desjardins-Carrière, F. Lapointe, P. Gagnon, F. L. Larouche, E. Adam, M. Paillet, and R. Martel, J. Electrochem. Soc. **1201** 1211 (2012).
[51] R.S. Knox, *Theory of Excitons*, Solid State Physics Suppl. 5 (Academic Press, New York, 1963).
[52] V. Perebeinos, J. Tersoff, and P. Avouris, Phys. Rev. Lett. **92**, 257402 (2004).
[53] J. Jiang, R. Saito, G. G. Samsonidze, A. Jorio, S. G. Chou, G. Dresselhaus, and M. S. Dresselhaus, Phys. Rev. B **75**, 035407 (2007).
[54] M. Rohlfing and S. G. Louie, Phys. Rev. B **62**, 4927 (2000).

[55] One can use the same model and part the assumption of electron-hole symmetry (to be discussed elsewhere), in which case some of the simplifications used below will not be applicable.
[56] J. J. Crochet, J. D. Sau, J. G. Duque, S. K. Doorn, and M. L. Cohen, ACS Nano, **5**, 2611 (2011).
[57] Ph. Avouris, M. Freitag, and V. Perebeinos, *Carbon Nanotube Optoelectronics*, Topics in Appl. Phys. **111**, 423 (2008).
[58] H. Haug and S. W. Koch, *Quantum Theory of the Optical and Electronic Properties of Semiconductors* (World Scientific, Singapore, 2004).
[59] M. F. Islam, D. E. Milkie, C. L. Kane, A.G. Yodh, and J.M. Kikkawa, Phys. Rev. Lett. **93**, 037404 (2004).